Journal of Nuclear Materials 396 (2010) 94–101

Contents lists available at ScienceDirect

Journal of Nuclear Materials

journal homepage: www.elsevier.com/locate/jnucmat

# Structural investigations of borosilicate glasses containing $MoO_3$ by MAS NMR and Raman spectroscopies

D. Caurant [a,*], O. Majérus [a], E. Fadel [a], A. Quintas [a], C. Gervais [b], T. Charpentier [c], D. Neuville [d]

[a] Laboratoire de Chimie de la Matière Condensée de Paris, UMR-CNRS 7574, Ecole Nationale Supérieure de Chimie de Paris (ENSCP, ParisTech), 11 rue Pierre et Marie Curie, 75231 Paris, France
[b] Laboratoire de Chimie de la Matière Condensée de Paris, UMR-CNRS 7574, Université Pierre et Marie Curie, 75252 Paris, France
[c] CEA, IRAMIS, Service Interdisciplinaire sur les Systèmes Moléculaires et Matériaux, CEA Saclay, 91191 Gif-sur-Yvette, France
[d] Physique des Minéraux et des Magmas, UMR-CNRS 7047, Institut de Physique du Globe, place Jussieu, 75252 Paris, France

ARTICLE INFO

*Article history:*
Received 26 February 2009
Accepted 22 October 2009

ABSTRACT

High molybdenum concentration in glass compositions may lead to alkali and alkaline-earth molybdates crystallization during melt cooling that must be controlled particularly during the preparation of highly radioactive nuclear glassy waste forms. To understand the effect of molybdenum addition on the structure of a simplified nuclear glass and to know how composition changes can affect molybdates crystallization tendency, the structure of two glass series belonging to the $SiO_2$–$B_2O_3$–$Na_2O$–$CaO$–$MoO_3$ system was studied by $^{29}Si$, $^{11}B$, $^{23}Na$ MAS NMR and Raman spectroscopies by increasing $MoO_3$ or $B_2O_3$ concentrations. Increasing $MoO_3$ amount induced an increase of the silicate network reticulation but no significant effect was observed on the proportion of $BO_4^-$ units and on the distribution of $Na^+$ cations in glass structure. By increasing $B_2O_3$ concentration, a strong evolution of the distribution of $Na^+$ cations was observed that could explain the evolution of the nature of molybdate crystals ($CaMoO_4$ or $Na_2MoO_4$) formed during melt cooling.



## 1. Introduction

Spent nuclear fuel reprocessing generates highly radioactive liquid wastes (HLW) with high Mo concentration that are currently immobilized in borosilicate glass matrices containing both alkali and alkaline-earth elements [1,2]. Because of its high field strength, $Mo^{6+}$ cation has a limited solubility in silicate and borosilicate glasses and crystallization of alkali or alkaline-earth molybdates may occur during melt cooling or heat treatment of glasses [3–5]. Indeed, according to EXAFS results giving the average Mo–O distance $d$(Mo–O) in silicate and borosilicate glasses [1,6–8], the field strength $F$ of $Mo^{6+}$ cation ($F = 6/d(\text{Mo–O})^2$) ranges between 1.89 and 1.935 $Å^{-2}$ (Table 1). Consequently, $Mo^{6+}$ cation exerts a strong ordering effect on the surrounding oxygen anions and may easily separate from the silicate or borosilicate glassy network combining with other elements such as alkali and alkaline-earth cations to form crystalline molybdates. The crystallization of poorly durable Mo-rich phases such as the complex "yellow phases" containing water soluble alkali molybdates that could incorporate significant amounts of radioactive cesium may thus occur during melt cooling of Mo-rich glass compositions. Consequently, even if Mo is not a radioactive fission product (all the Mo isotopes occurring in HLW solutions are non-radioactive), the formation of these "yellow phases" must be avoided during nuclear glasses preparation because this would lead to waste forms with lower long term performances than homogeneous glasses due to the increase of the leaching rate of the short-lived $^{137}Cs$ and long-lived $^{135}Cs$ radioactive isotopes if the waste forms come into contact with water during storage or disposal. Nevertheless, the higher chemical durability of $CaMoO_4$ in comparison with alkali molybdates such as $Na_2MoO_4$ (according to [9] the solubility of $Na_2MoO_4$ in water is more than three orders of magnitude higher than that of $CaMoO_4$ at room temperature and (Ca,Sr,Ba)$MoO_4$ was the phase envisaged to immobilize Mo, Sr and Ba fission products in the multiphase supercalcine ceramics studied in 1970s for HLW conditioning [10]) recently enabled to envisage a glass composite waste form consisting of a vitreous phase as major component with Mo-rich spherical particles – containing $CaMoO_4$ crystals – dispersed uniformly in the vitreous phase and formed during melt cooling after casting in metallic canisters [11,12]. This waste form – referred to as SUMo2-12c [11] – has been developed to immobilize old waste solutions with high Mo concentration recovered in 1970s after the reprocessing of UMo spent fuel that was used in gas cooled reactors in 1960s in France [11].

In this paper, we present structural results obtained on a simplified glass composition derived from this waste form and belonging to the $SiO_2$–$Na_2O$–$CaO$–$B_2O_3$–$MoO_3$ system. In a recent work on

* Corresponding author. Tel.: +33 153767922; fax: + 33 146347489.
*E-mail address:* daniel-caurant@enscp.fr (D. Caurant).

0022-3115/$ - see front matter © 2009 Elsevier B.V. All rights reserved.
doi:10.1016/j.jnucmat.2009.10.059

**Table 1**
Average distance d(Mo–O) between $Mo^{6+}$ cation and its first oxygen neighbors deduced from Mo–K edge EXAFS experiments performed on Mo-bearing glass compositions belonging to the $SiO_2$–$Na_2O$–$K_2O$ [8] and $SiO_2$–$Na_2O$ [7] systems and on Mo-bearing inactive borosilicate nuclear glasses [1,6]. The field strength $F$ defined as $F = Z/d(Mo–O)^2$ with $Z$ the cation charge and $d$(Mo–O) in Å units was calculated. The bond valence $S_{Mo–O}$ (in valence units, v.u.) of the Mo–O bonds was calculated from Mo EXAFS results according to the formula $S_{Mo–O} = \exp[(R_0 - d(Mo–O))/b]$, where $R_0$ is the bond valence parameter of $Mo^{6+}$ cation ($R_0(Mo^{6+}) = 1.907$ Å) and $b$ is a constant ($b = 0.37$ Å) [40]. The sum of the bond valences $S_{Mo–O} + S_{Si–O}$ of Mo–O and Si–O bonds for hypothetic Mo–O–Si linkages is also given assuming that $S_{Si–O} = 1.10$ v.u. [18].

| $d$(Mo–O) in Å | Field strength in $Å^{-2}$ | Bond valence ($S_{Mo–O}$) in v.u. | $S_{Mo–O} + S_{Si–O}$ in v.u. | References |
|---|---|---|---|---|
| 1.78 | 1.89 | 1.41 | 2.51 | [1] |
| 1.76 | 1.935 | 1.49 | 2.59 | [7] |
| 1.77 | 1.91 | 1.45 | 2.55 | [8] |
| 1.76 | 1.935 | 1.49 | 2.59 | [6] |

this system [5], we showed that glass composition changes can significantly modify the nature and the relative proportions of the molybdate crystals that may form during natural cooling of the melt at 1 °C/min (i.e. at a rate close to the average cooling rate of the bulk of borosilicate nuclear melts in metallic canisters during the first 10 h after casting). For instance, it appeared that $CaMoO_4$ crystallization tendency increased at the expenses of $Na_2MoO_4$ when $B_2O_3$ concentration increased. Thus, by changing glass composition, we showed that it was possible to orientate the glass crystallization tendency towards a more chemically durable phase. We present here structural results on two series of quenched glasses ($M_x$ and $B_y$ series) melted in air and belonging to the previous system using $^{29}Si$, $^{11}B$, $^{23}Na$ MAS NMR and Raman spectroscopies. The effect of increasing $MoO_3$ concentration on the glass network structure is studied ($M_x$ series). The evolution of the distribution of $Na^+$ cations within the borosilicate network is followed when either $B_2O_3$ ($B_y$ series) or $MoO_3$ ($M_x$ series) concentrations increases and is discussed according to the evolution of the crystallization tendency of the melt during controlled cooling at 1 °C/min [5]. Raman spectroscopy is used to follow the evolution of molybdenum environment (present as $MoO_4^{2-}$ units) in glass structure with composition changes.

## 2. $Mo^{6+}$ cations in silicate and borosilicate glasses structure

When silicate and borosilicate glasses are prepared under oxidizing or neutral atmosphere, molybdenum mainly occurred at oxidation state +VI which is the most stable oxidation state of molybdenum in these conditions [3,13–15]. According to Mo EXAFS and XANES results [1,8,6,7] obtained for silicate and borosilicate glasses containing $Mo^{6+}$ cations, these cations would be present in tetrahedral sites as molybdate $MoO_4^{2-}$ entities. Using the average $d$(Mo–O) distance determined by Mo EXAFS (Table 1) and bond valence considerations [16] derived from Pauling's stability rules [17], it was shown that $MoO_4^{2-}$ entities cannot be directly connected to the silicate network [18]. Indeed, the existence of Mo–O–Si linkages between $MoO_4$ and $SiO_4$ tetrahedra would imply that the sum of the bond valences $S_{Mo–O} + S_{Si–O} \approx 2.5$–2.6 valence units (v.u.) > 2 v.u. for the oxygen atom between Mo and Si (Table 1) which is not possible according to Pauling's stability rules because in such a situation the oxygen atom would be strongly overbonded. Consequently, the only charge compensating cations that can be found around molybdate entities in silicate glasses structure to stabilize their negative charge should be alkali or alkaline-earth cations (but not silicon or other glass former cations). According to these structural results it can be proposed that in borosilicate glasses, molybdate entities are located in depolymerized regions of the glass structure (i.e. in non-bridging oxygen atoms (NBOs)-rich regions) containing alkali and alkaline-earth cations to compensate their negative charge [1,7] (Fig. 1). The presence of high contents of both molybdenum and alkali or alkaline-earth cations in the same regions of the glass structure may explain the rather high crystallization tendency of alkali or alkaline-earth molybdate crystalline phases during melt cooling or heat treatment above the glass transformation temperature. Indeed, the same kind of isolated $MoO_4^{2-}$ tetrahedral entities (Fig. 1) are present for instance in both $Na_2MoO_4$ (spinel structure, Fig. 2a) and $CaMoO_4$ (scheelite structure, Fig. 2b) phases that can crystallize in nuclear borosilicate glasses. The similarity between the local environment of $Mo^{6+}$ cations in glasses and in molybdate crystalline phases may thus explain the low solubility of molybdenum in

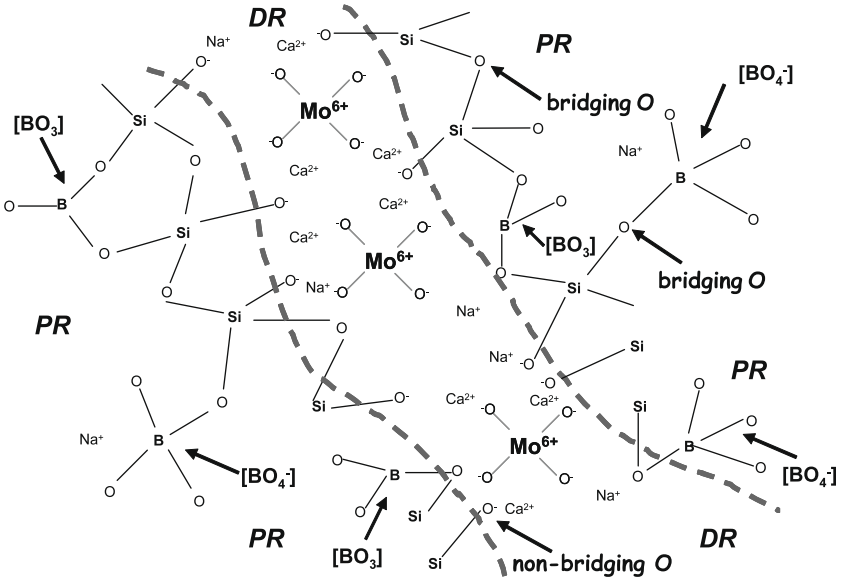


**Fig. 1.** Schematic representation of the structure of a soda-lime borosilicate glass containing molybdenum according both to Mo EXAFS results reported in literature [1,7,18] and to the modified random network model of the structure of modified silicate glasses [41]. In this figure are shown: $(MoO_4)^{2-}$ entities no directly connected to the borosilicate network but located in depolymerized regions of the glass structure, $SiO_4$ tetrahedra, $BO_4$ tetrahedral units that can be charge compensated by $Na^+$ or $Ca^{2+}$ cations, $BO_3$ triangles. Examples of bridging oxygen atoms (BOs) and non-bridging oxygen atoms (NBOs) are shown. The possible presence of Si and B in the neighborhood of $MoO_4^{2-}$ units – as second neighbors of the $Na^+$ or $Ca^{2+}$ cations that charge compensate the molybdate units – is proposed in the figure. DR: depolymerized regions (i.e. regions rich in both NBOs and $Na^+ + Ca^{2+}$ cations); PR: polymerized regions (i.e. NBOs-poor regions). The dotted lines separate DR and PR regions.

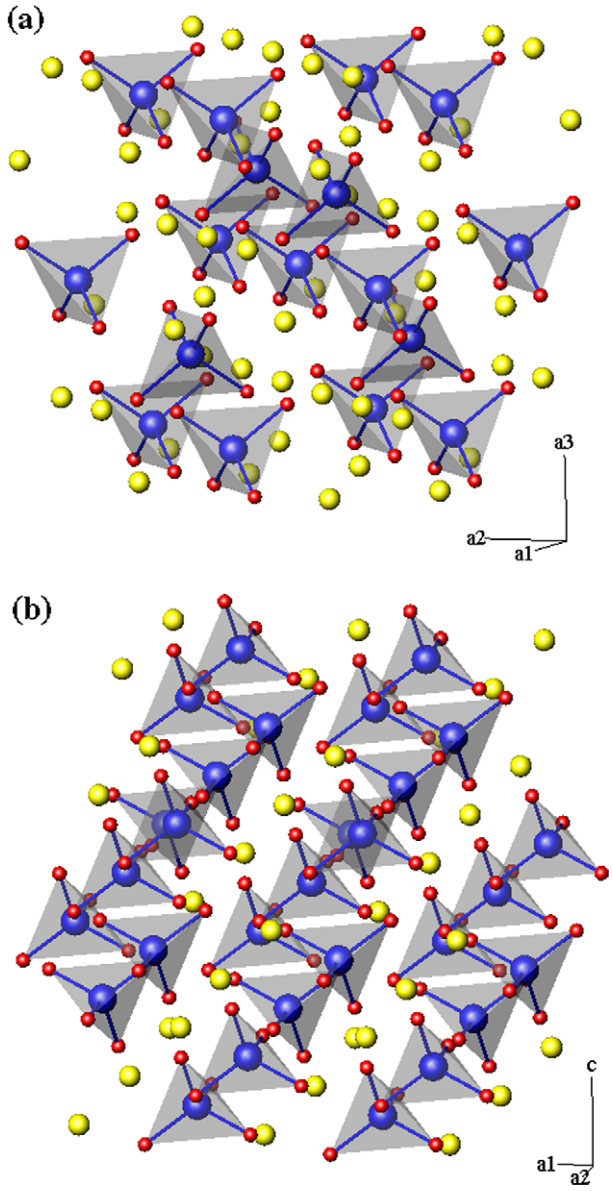


**Fig. 2.** Structure of $Na_2MoO_4$ (a) and $CaMoO_4$ (b) crystalline phases. At room temperature (until about 400–460 °C), the stable form of $Na_2MoO_4$ has a spinel structure ($a_1 = a_2 = a_3$) in which $Mo^{6+}$ cations form tightly bound molecular $MoO_4^{2-}$ entities which are bounded to the $Na^+$ cations located in octahedral sites. In this structure, the $MoO_4^{2-}$ entities are not directly connected one to another and remain isolated in the $Na^+$ cations lattice. $CaMoO_4$ (powellite) has the tetragonal scheelite ($CaWO_4$) structure ($a_1 = a_2 \neq c$). In scheelite, $Mo^{6+}$ cations also form tightly bound molecular $MoO_4^{2-}$ entities which are bounded to the $Ca^{2+}$ cations (located in 8-fold coordinated sites) in the lattice via relatively weak long-range ionic forces. Similarly to $Na_2MoO_4$, in powellite the $MoO_4^{2-}$ entities are not directly connected one to another and remain isolated in the $Ca^{2+}$ cations lattice. Contrary to $MoO_4$ tetrahedra in $Na_2MoO_4$ that are almost perfect (with all (O–Mo–O) angles ~109° [42]), $MoO_4$ tetrahedra in $CaMoO_4$ are rather distorted. However, $CaMoO_4$ structure remains stable with temperature (only one allotropic form is reported in molybdates phase diagrams [43,44]) which is not the case for $Na_2MoO_4$. Blue spheres: $Mo^{6+}$ cations. Yellow spheres: $Na^+$ (a) or $Ca^{2+}$ (b) cations. Red spheres: $O^{2-}$ anions. In the figure, spheres size is not related to ionic radii (For interpretation of the references to colour in this figure legend, the reader is referred to the web version of this article.).

glasses and its tendency to lead to crystallization during cooling of melts or heat treatment of glasses. The fact that $Mo^{6+}$ cations are far more soluble in phosphate glasses (for instance in the $P_2O_5$–$MoO_3$ system, glasses can be prepared with a $MoO_3$ concentration ranging from 0 to ~83 mol% [19]) than in silicate glasses could be explained by the fact that molybdenum cations would be mainly present in six-coordinated environment and would be connected to the phosphate network [19–22].

Let us now consider different spectroscopic methods that can be used to check directly the environment of $Mo^{6+}$ cations in glasses. The study of the average Mo–O distances determined by Mo EXAFS spectroscopy of various $Mo^{6+}$-bearing silicate and borosilicate glasses shows that $d$(Mo–O) remains almost constant (1.76–1.78 Å) whatever the glass composition [1,8,6,7] (Table 1). This observation suggests that Mo EXAFS spectroscopy is probably not sensitive enough to detect the effect of glass composition changes on the environment of molybdenum cations in silicate and borosilicate glasses. In comparison, other techniques such as Raman and $^{95}$Mo MAS NMR spectroscopies can be very helpful to study the variation of $MoO_4^{2-}$ environment with glass composition. Indeed, these techniques are respectively sensitive to the variation of the molybdate entities vibration frequency and to the variation of the interaction between the nuclear spin associated with $^{95}$Mo nuclei and their neighborhood.

Concerning Raman spectroscopy, several authors indicated that the frequency of the Mo–O symmetric stretching vibration of $MoO_4^{2-}$ tetrahedral units in crystalline phases was sensitive to their composition [23,24]. Indeed, the existence of a correlation between the Raman stretching frequency $\nu_{Mo-O}$ of Mo–O bonds and the $d$(Mo–O) distance in a large number of molybdate crystalline compounds showing that the frequency decreased non linearly with the bond length was reported by Hardcastle and Wachs [24]: $\nu_{Mo-O}$ in $cm^{-1}$ = 32,895 exp(−2.073 $d$(Mo–O)). Nevertheless, to the best of our knowledge, Raman studies have not yet been reported in literature on Mo-bearing silicate glasses to follow the evolution of the vibration bands associated with molybdate entities by changing glass composition. In the present work performed on Mo-bearing silicate and borosilicate glasses, we show that Raman spectroscopy is sensitive to study the variation of $MoO_4^{2-}$ units environment in glass structure.

Concerning $^{95}$Mo MAS NMR spectroscopy, it is known that $^{95}$Mo is difficult to detect by NMR because of both its low gyromagnetic ratio in comparison with other nuclei classically studied in oxide glasses ($^{29}$Si, $^{27}$Al, $^{11}$B, $^{31}$P, $^{23}$Na) and its low natural abundance (15.92%). Moreover, as $^{95}$Mo is a quadrupolar nucleus ($I$ = 5/2), second-order quadrupolar broadening occurs on MAS NMR spectra. Despite these difficulties, it has been recently shown that $^{95}$Mo MAS NMR can enable to probe directly $Mo^{6+}$ cations cations in silicate and borosilicate glasses and may prove useful in understanding the impact of composition changes on glass structure by following the evolution of $^{95}$Mo chemical shift [25,26]. Nevertheless, in the present paper only Raman spectroscopy was used to study the evolution of molybdenum environment in our glass samples.

## 3. Glass preparation and characterization methods

Two series of glasses $M_x$ and $B_y$ were prepared for this study, all derived from the following composition (in mol%): 58.2 $SiO_2$–13.77 $Na_2O$–9.81 CaO–18.08 $B_2O_3$ either by increasing $MoO_3$ concentration from 0 to 5.0 mol% ($M_x$ series with $x$ = 0, 0.87, 1.54, 2.50, 3.62, 5 mol%) or by changing $B_2O_3$ concentration from 0 to 24 mol% ($B_y$ series with $y$ = 0, 6, 12, 18, 24 mol%) while maintaining a constant $MoO_3$ concentration (2.50 mol%). For all samples, 0.15 mol% $Nd_2O_3$ was introduced in the composition both to facilitate $^{29}$Si nuclei relaxation during MAS NMR experiments and to perform optical studies not presented in this paper [5]. Glasses were all prepared at 1300 °C in air in Pt crucibles using reagent grade $SiO_2$, $CaCO_3$, $Na_2CO_3$, $H_3BO_3$, $MoO_3$ and $Nd_2O_3$ powders. Depending on glass composition, samples were quenched either as cylinders or disks without annealing [5]. In spite of the high

$B_2O_3$ content in the compositions studied in this work no phase separation was detected by SEM for the samples without $MoO_3$ ($M_0$ sample). The separation of very small globular particles was only detected when the $MoO_3$ content exceeds 2.5 mol% [5]. Thus, it appears that in the system studied here the phase separation is only induced by the addition of significant amount of molybdenum oxide. Several borate and silicate reference glass samples whose compositions are given in the captions of Figs. 4 and 7 were also prepared for comparison with $M_x$ and $B_y$ glasses by MAS NMR and Raman spectroscopies. The amorphous character of all samples was checked using both X-ray diffraction (XRD) and Raman spectroscopy. XRD characterization was performed by the help of a Siemens D5000 apparatus operating at Co $K_\alpha$ wavelength ($\lambda$ = 1.778897 Å). Unpolarized Raman spectra were collected at room temperature on a T64000 Jobin–Yvon confocal Raman spectrometer equipped with a CCD detector cooled by nitrogen. The 488 nm line of a Coherent 70 $Ar^+$ laser was used as the excitation source.

$^{29}Si$, $^{11}B$ and $^{23}Na$ MAS NMR spectra were recorded respectively at 59.63, 128.28 and 132.03 MHz. Chemical shifts were determined relative to tetramethylsilane for $^{29}Si$, liquid $BF_3OEt_2$ for $^{11}B$ and a 1.0 M aqueous NaCl solution for $^{23}Na$. The $^{23}Na$ MAS NMR data were processed using a homemade program to fit the spectra by taking into account the effects of the parameter distribution for both the quadrupolar interaction and the isotropic chemical shift, as described in [27]. In this case, very satisfactory results were obtained using a Gaussian isotropic model for the quadrupolar interaction [28,29] and a normal distribution for the isotropic chemical shift. This fitting procedure provides the mean value of the isotropic chemical shift $\delta_{iso}$ and the mean value of the quadrupolar coupling parameter Pq.

For all glasses, ESR was used to investigate the occurrence of paramagnetic $Mo^{5+}$ ($4d^1$) or $Mo^{3+}$ ($4d^3$) cations and spectra were recorded at *X* band (9.5 GHz) between 20 and 300 K. For all glasses of $M_x$ and $B_y$ series, ESR spectra revealed the existence of a signal due to molybdenum centered near $g \sim 1.913$ and detected from 20 K to room temperature (Fig. 3a). No signal associated with $Mo^{3+}$ ($4d^3$) cations near $g \sim 5.19$ was observed [7,30]. The characteristics of the ESR signal indicated that it could be attributed to $Mo^{5+}$ cations located in low symmetry sites as the spin–lattice relaxation time of $d^1$ ions is known to increase with site distortion enabling to detect their ESR signals at high temperature [31]. The presence of a small intensity hyperfine structure on EPR spectra (Fig. 3a), that can be attributed to the contribution of $^{95}Mo$ and $^{97}Mo$ isotopes with nuclear spin $I = 5/2$, confirmed that the signal at $g = 1.913$ was due to molybdenum and no to other paramagnetic impurities. Moreover, the nearly linear intensity increase of the EPR signal with $MoO_3$ content in $M_x$ glasses (Fig. 3b) also confirmed that the spectrum was due to molybdenum. It is also interesting to note that, as no evolution of the linewidth of the EPR signal (~28 G) was observed with increase in $MoO_3$ concentration even for the highest concentrated samples (5 mol% $MoO_3$), the magnetic interactions between paramagnetic molybdenum cations remain small. This indicates that $Mo^{5+}$ cations are diluted rather than aggregated in the glassy network. The proportion of $Mo^{5+}$ cations (over all molybdenum) ranges between 0.4% and 0.8% for all the glasses studied in this work as estimated using a DPPH sample as concentration standard. Consequently, the majority of molybdenum (>99%) occurs as $Mo^{6+}$ cations in all glasses of the $M_x$ and $B_y$ series prepared in this study (oxidizing conditions). Thus, according to Mo EXAFS and XANES results published in literature on silicate and borosilicate glasses [1,7,8] and to bond valence considerations [16], it can be assumed that the majority of molybdenum cations in our glasses are present as tetrahedral $MoO_4^{2-}$ molybdate entities in modifiers-rich (i.e. depolymerized) regions of the glass structure and are not linked directly to the silicate network (Fig. 1).

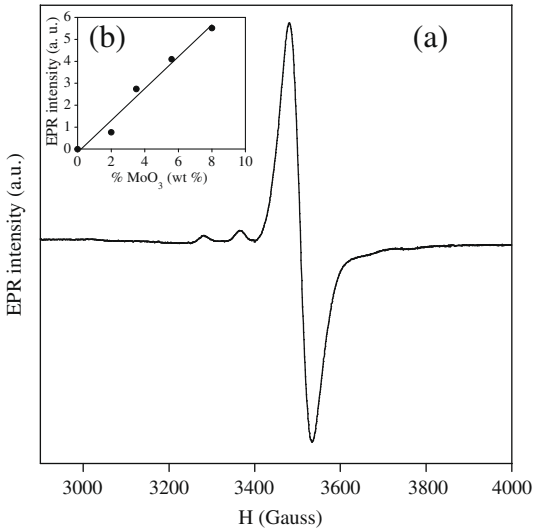


**Fig. 3.** EPR spectrum (a) of $Mo^{5+}$ cations in $M_{2.5}$ glass (2.5 mol% $MoO_3$) recorded at room temperature (*X*-band, 9.51 GHz). The intense EPR signal centered near $g = 1.913$ arises from the even Mo isotopes ($I = 0$, natural abundance 74.62%) and the smaller lines detected at lower magnetic field (between 3200 and 3400 G in the figure) arise from the hyperfine structure from odd $^{95}Mo$ ($I = 5/2$, natural abundance 15.78%) and $^{97}Mo$ ($I = 5/2$, natural abundance 9.60%) isotopes. The evolution of the global intensity (obtained by double integration of the EPR signal) versus $MoO_3$ concentration (in wt.%) for all glasses of the $M_x$ series is shown in (b) with a linear fit.

## 4. Structural evolution of glasses with increasing $MoO_3$ concentration

Raman spectra confirms the XRD results presented in [5] showing that the solubilty limit of molybdenum in $M_x$ glasses was reached between 1.54 and 2.5 $MoO_3$ mol%. Indeed, Fig. 4 clearly reveals the occurrence of the contribution of $CaMoO_4$ (powellite)

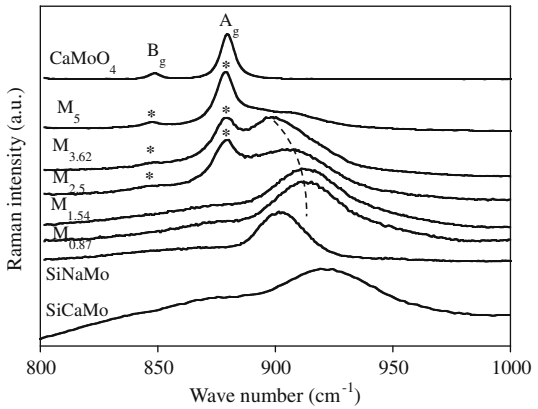


**Fig. 4.** Normalized Raman spectra of $M_{0.87}$, $M_{1.54}$, $M_{2.5}$, $M_{3.62}$ and $M_5$ glasses. The spectra of a $CaMoO_4$ (powellite) ceramic sample and of two reference sodium silicate and calcium silicate glasses containing molybdenum and referred respectively to as SiNaMo ($69.34SiO_2$–$28.09Na_2O$–$2.43MoO_3$–$0.15Nd_2O_3$ in mol%) and SiCaMo ($58.89SiO_2$–$40.15CaO$–$0.82MoO_3$–$0.15Nd_2O_3$ in mol%) are also given for comparison. ∗: Vibration bands due to $CaMoO_4$ crystals in $M_x$ samples. For the $M_5$ sample, XRD revealed the presence of a low amount of small γ-$Na_2MoO_4$ crystals [5] whose contribution is not observed on the Raman spectra. The dotted line is a guide for the eye to follow the evolution of the maximum of the band associated with molybdates entities in glasses. Spectra have not been corrected for temperature and frequency dependent scattering intensity [45].

Raman vibration modes when $x > 1.54$ mol% (i.e. 3.5 wt.%). For comparison, the Raman spectrum of a powellite ceramic sample is given with bands attribution according to [32]. All the $CaMoO_4$ vibration bands with frequency $\geqslant 321\ cm^{-1}$ correspond to internal vibrational modes of $MoO_4^{2-}$ tetrahedra and the strongest band $A_g$ at $879\ cm^{-1}$ is associated with the symmetric stretching vibration of Mo–O bonds. By analogy, we propose that the wide and intense band observed in the 898–913 $cm^{-1}$ range of the Raman spectra for all glasses of $M_x$ series (and also for those of the $B_y$ series) is also due to the symmetric stretching vibration of Mo–O bonds of molybdate tetrahedra within the glass structure. We saw above that Hardcastle and Wachs [24] reported an empirical correlation between the Raman stretching frequency of Mo–O bonds and the d(Mo–O) bond length for several crystalline molybdates showing the sensitivity of this frequency to $MoO_4^{2-}$ environment. Nevertheless, other authors [33] indicated that the energy of the Raman Mo–O stretching frequency also depended on $MoO_4^{2-}$ tetrahedra distortion in crystalline samples. Thus, it seems difficult to simply correlate the shift of the Raman band with $MoO_4^{2-}$ tetrahedra structural parameters for the glasses studied in this work. Nevertheless, Fig. 4 clearly demonstrates that this band shifted towards lower frequencies when $x$ increases ($x \geqslant 2.5$ mol%) which shows that the environment and/or the symmetry of $MoO_4^{2-}$ tetrahedra in the glass is modified when crystallization of powellite is detected ($x > 1.54$ mol%). For comparison, spectra of two reference glasses belonging to the $SiO_2$–$Na_2O$–$MoO_3$ (SiNaMo glass) and $SiO_2$–CaO–$MoO_3$ (SiCaMo glass) systems and for which all the $MoO_4^{2-}$ entities are charge compensated by $Na^+$ and $Ca^{2+}$ cations respectively are also shown in Fig. 4. For these two glasses, the frequency of the symmetric stretching vibration of Mo–O bonds of molybdate tetrahedra are significantly different: SiNaMo (902 $cm^{-1}$), SiCaMo (922 $cm^{-1}$). This shows that Raman spectroscopy is sensitive to the nature of the cations that charge compensate molybdate entities in silicate glasses. The band shift towards lower energies observed in Fig. 4 when $MoO_3$ content increases could thus indicate that the proportion of $MoO_4^{2-}$ tetrahedra charge compensated by $Na^+$ cations increases with $x$ at the expenses of $MoO_4^{2-}$ tetrahedra charge compensated by $Ca^{2+}$ cations when $CaMoO_4$ begun to crystallize. This evolution could be explained by an increase of the Na/Ca ratio in the modifiers-rich regions of glass structure when powellite is formed. For $M_{0.87}$ and $M_{1.54}$ glasses, the maximum of the Mo–O symmetric stretching band (913 $cm^{-1}$) is intermediate between that of the two reference glasses suggesting that when $x < 2.5$ mol%, $MoO_4^{2-}$ tetrahedra are charge compensated both by $Na^+$ and $Ca^{2+}$ cations.

$^{29}Si$ MAS NMR spectra were all simulated with the DMFIT program [34] using three bands centered at −80.0, −92.2 and −103.6 ppm respectively attributed to $Q_2$, $Q_3$ and $Q_4$ units ($Q_n$ units with $n$ = 0–4 correspond to $SiO_4$ tetrahedra with n bridging oxygen atoms). An example of curve-fitting is shown in Fig. 5a and the evolution of the relative proportions $[Q_n]$ of $Q_n$ units is shown in Fig. 5b. This evolution reveals that $[Q_2]$ and $[Q_3]$ decrease whereas $[Q_4]$ increases when molybdenum concentration increases in samples of the $M_x$ series. When $MoO_3$ content increases from 0 to 5 mol% the proportion of $Q_4$ units increases of more than 20% (Table 2). The observation of a slight increase of the intensity of $Q_4$ units contribution on Raman spectra near 1100–1200 $cm^{-1}$ between $M_0$ and $M_5$ samples (spectra not shown) confirmed $^{29}Si$ NMR results. For the $M_x$ series, $^{11}B$ MAS NMR spectra simulation only shows a slight and no monotonous decrease of the relative proportion of $BO_4^-$ units when molybdenum concentration increases. The variation of the proportion of $BO_4^-$ units is only about 2–4% (Table 2). Consequently in $M_x$ glasses, $MoO_3$ acts as a reticulating agent for the silicate network and it mainly acts on the amount of $Q_3$ units (Table 2). This result can be explained as follows. As molybdenum is introduced as $MoO_3$ (corresponding to one $Mo^{6+}$ cation and three NBOs) in glass batch whereas $Mo^{6+}$ cations are known to occur as $MoO_4^{2-}$ units (corresponding to one $Mo^{6+}$ cation and four NBOs) both in glass structure and in powellite crystals, each $Mo^{6+}$ cation introduced in the composition needs to catch one NBO more from the borosilicate network. We thus propose the following reaction scheme between $MoO_3$ and $Q_3$ units (initially charge compensated by $Na^+$ or $Ca^{2+}$ cations) in the melt:

$$MoO_3 + (2Q_3,\ Ca^{2+} \text{ or } 2Na^+) \rightarrow (MoO_4^{2-},\ Ca^{2+} \text{ or } 2Na^+) + 2Q_4. \quad (1)$$

For a constant number of moles of $SiO_2$ (58.2 in $M_0$ composition), the number of moles of $Mo^{6+}$ cations ($n_{Mo}$) and $Q_3$ units ($n_{Q_3}$) was calculated for all $M_x$ samples and is reported in Table 2. The comparison of $|\Delta n_{Q_3}|$ (the number of moles of $Q_3$ units that have disappeared in $M_x$ sample in comparison with $M_0$ sample) with $2n_{Mo}$ (see Eq. (1)) shows that the values of $|\Delta n_{Q_3}|$ and $2n_{Mo}$ remains close to each other when the amount of $MoO_3$ increases in glass composition which seems to confirm the reaction scheme (1).

Experimental and simulated $^{23}Na$ MAS NMR spectra of glasses of the $M_x$ series are shown in Fig. 6a and the evolution of the mean isotropic chemical shift ($\delta_{iso}$) and quadrupolar coupling parameter ($P_Q$) deduced from spectra simulation is shown in Fig. 7. As $^{23}Na$ NMR parameters $\delta_{iso}$ and $P_Q$ are very sensitive to sodium environment both in glass and crystalline structures [35], the fact that the

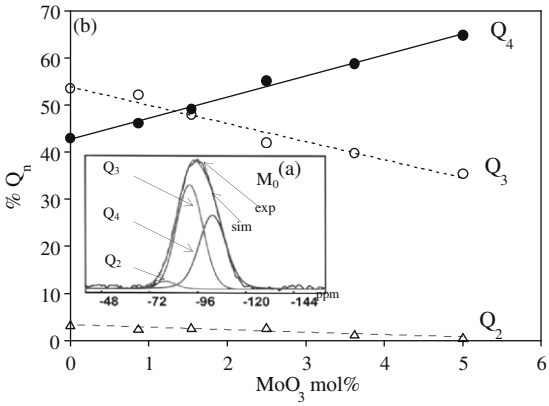


**Fig. 5.** (a) Example of $^{29}Si$ MAS NMR spectra recorded for the $M_0$ sample. The corresponding simulation using three Gaussian line shape contributions associated with $Q_2$, $Q_3$ and $Q_4$ units is shown (exp: experimental spectrum, sim: simulated spectrum). The same chemical shift values were used for the spectra simulation of all the samples of $M_x$ and $B_y$ series. (b) Evolution of the relative proportions of $Q_4$, $Q_3$ and $Q_2$ units in $M_x$ samples with the increase of $MoO_3$ concentration. Linear fits of $Q_n$ evolution are shown.

**Table 2**
Relative proportions of $Q_n$ units ($n$ = 2, 3, 4) and of $BO_3$ and $BO_4^-$ units in $M_x$ samples determined after simulation and integration of $^{29}Si$ and $^{11}B$ MAS NMR spectra with the DMFIT program [34]. For a constant number of moles of $SiO_2$ (58.2 in $M_0$ composition), the number of moles of $Mo^{6+}$ cations ($n_{Mo}$) and $Q_3$ units ($n_{Q_3}$) is reported for all $M_x$ samples. The number of moles of $Q_3$ units that disappeared ($|\Delta n_{Q_3}|$) when $x$ increased (in comparison with $M_0$ glass) is also reported.

| | $M_0$ | $M_{0.87}$ | $M_{1.54}$ | $M_{2.50}$ | $M_{3.62}$ | $M_5$ |
|---|---|---|---|---|---|---|
| % $Q_4$ | 43 | 46.2 | 49.2 | 55.2 | 58.8 | 64.8 |
| % $Q_3$ | 53.6 | 52.2 | 48.0 | 42.0 | 39.8 | 34.5 |
| % $Q_2$ | 3.4 | 2.6 | 2.8 | 2.8 | 1.4 | 0.7 |
| $n_{Q_3}$ | 31.19 | 30.38 | 27.93 | 24.44 | 23.16 | 20.08 |
| $n_{Mo}$ | 0 | 0.87 | 1.56 | 2.56 | 3.75 | 5.26 |
| $\lvert\Delta n_{Q_3}\rvert$ | – | 0.81 | 3.26 | 6.75 | 8.03 | 11.11 |
| $2n_{Mo}$ | 0 | 1.74 | 3.12 | 5.12 | 7.5 | 10.52 |
| % $BO_3$ | 46.0 | 43.8 | 46.4 | 47.8 | 49.7 | 47.8 |
| % $BO_4$ | 54.0 | 56.2 | 53.6 | 52.3 | 50.3 | 52.3 |
| $[BO_4]/[BO_3]$ | 1.17 | 1.28 | 1.15 | 1.09 | 1.01 | 1.09 |

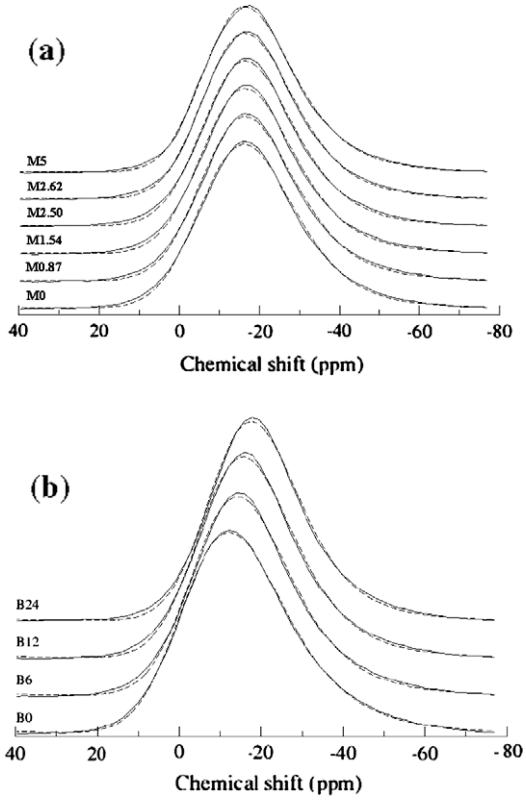


**Fig. 6.** $^{23}$Na MAS NMR spectra of glasses of $M_x$ (a) and $B_y$ (b) series (solid lines: experimental spectra, dashed lines: simulated spectra). The evolution of the mean isotropic chemical shift ($\delta_{iso}$) and quadrupolar coupling parameter ($P_Q$) deduced from spectra simulation is shown in Fig. 7.

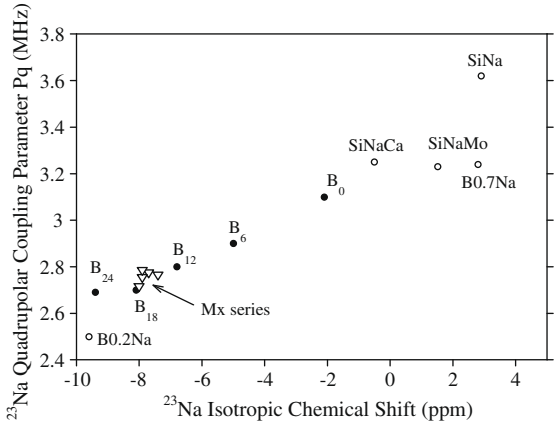


**Fig. 7.** Evolution of the mean isotropic chemical shift ($\delta_{iso}$) and quadrupolar coupling parameter ($P_Q$) of $^{23}$Na in samples of $B_y$ (●) and $M_x$ (∇) series deduced from the simulation of the spectra of Fig. 6. For comparison the values of $\delta_{iso}$ and $P_Q$ of reference glasses (○) are also shown (compositions in mol%): SiNa ($80.93SiO_2$–$19.07Na_2O$), SiNaCa ($71.21SiO_2$–$16.78Na_2O$–12CaO), B0.7Na ($58.8B_2O_3$–$41.2Na_2O$), SiNaMo ($69.34SiO_2$–$28.09Na_2O$–$2.43MoO_3$–$0.15Nd_2O_3$), B0.2Na ($83.3B_2O_3$–$16.7Na_2O$). In the four former reference glasses, $Na^+$ cations can compensate NBO whereas in B0.2Na glass $Na^+$ cations only compensate bridging oxygen atoms near $BO_4^-$ units.

mean $\delta_{iso}$ (~−7.83 ppm) and Pq (~2.74 MHz) parameters remains almost constant when $x$ increases (Fig. 7) shows that the mean environment of the majority of $Na^+$ cations does not change when molybdenum content increases. $BO_4^-$ entities being preferentially charge compensated by $Na^+$ cations rather than by $Ca^{2+}$ cations in borosilicate glasses [36], it can be deduced from $^{11}$B NMR results (Table 2) and $M_x$ glasses composition that about 70% of all the $Na^+$ cations could act as charge compensator near boron whereas the remaining $Na^+$ cations would be located near NBO or would charge compensated a fraction of the $MoO_4^{2-}$ tetrahedra. This could explain why the majority of sodium cations are not affected by increasing $MoO_3$ content.

In [5] we showed that $CaMoO_4$ was the only molybdate phase that crystallized during controlled cooling of the melt at 1 °C/min for compositions of the $M_x$ series for which $x > 3.5$ mol% $MoO_3$ whereas both $CaMoO_4$ and $Na_2MoO_4$ phases were detected in the quenched glass samples (cylinders and disks) when $x = 10.9$ mol% $MoO_3$. The fact that $Na_2MoO_4$ did not crystallize during slow cooling of $M_x$ samples from the melting to room temperature is probably due to the high $B_2O_3$ and CaO contents in their composition (respectively higher than 17 and 9 mol%). Indeed, because of both the preferential charge compensation of $BO_4^-$ units by $Na^+$ cations [36] and the relatively high CaO content in our glass compositions (in comparison for instance with the composition studied by Calas et al. [1] and for which $Na_2MoO_4$ is expected to crystallize during cooling of the melt), the high local Ca/Na concentration ratio of $Ca^{2+}$ and $Na^+$ cations around molybdate entities (Fig. 1) would favorize $CaMoO_4$ crystallization. The fact that a small amount of $Na_2MoO_4$ crystallized simultaneously with $CaMoO_4$ during rapid cooling of the $M_{10.9}$ melt but not during slow cooling at 1 °C/min [5] can be explained using the considerations developed by Calas et al. [1] on the temperature-induced coordination changes of boron: the boron partially changes from $BO_4$ to $BO_3$ coordination with increasing temperature. In this case, because of the preferential charge compensation of $(BO_4)^-$ units by $Na^+$ cations, during quenching of the $M_{10.9}$ melt the amount of $Na^+$ cations available to charge compensate molybdate entities (Fig. 1) would be higher (and thus also the local Na/Ca concentration ratio around molybdate entities) than during slow cooling and both $CaMoO_4$ and $Na_2MoO_4$ may crystallize.

## 5. Structural evolution of glasses with increasing $B_2O_3$ concentration

In [5] we showed that $Na_2MoO_4$ crystallization tendency during slow cooling of the melt (1 °C/min) decreased by increasing $B_2O_3$ concentration whereas the tendency of $CaMoO_4$ to crystallize increased. Such an evolution could be explained by the preferential charge compensation of $BO_4^-$ units by $Na^+$ [36]. Indeed, for $B_y$ series, Fig. 8 shows that $[BO_4^-]/[SiO_2]$ concentrations ratio increases whereas $[Na^+]/[BO_4^-]$ concentrations ratio decreases with $B_2O_3$

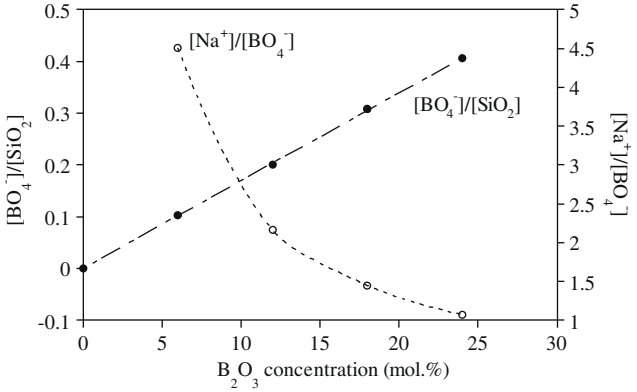


**Fig. 8.** Evolution of $[BO_4^-]/[SiO_2]$ and $[Na^+]/[BO_4^-]$ concentrations ratios versus $B_2O_3$ content in $B_y$ samples (in mol%). $[Na^+]$ and $[SiO_2]$ concentrations were determined by chemical analysis whereas $[BO_4^-]$ concentration was determined using both chemical analysis and $^{11}$B MAS NMR.

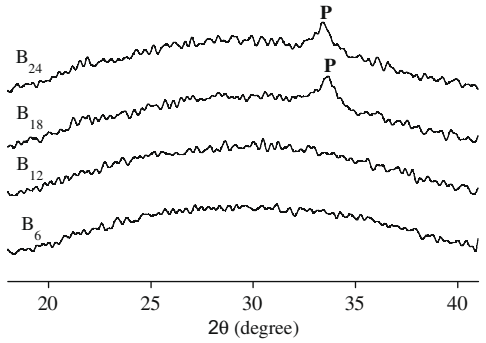


**Fig. 9.** XRD patterns of $B_y$ quenched disk samples. *P*: $CaMoO_4$ (powellite).

concentration and it is interesting to notice that for the $B_{24}$ sample almost all $Na^+$ cations can act as charge compensator of $BO_4^-$ units ($[Na^+]/[BO_4^-] \sim 1$). In these conditions, the amount of $Na^+$ cations able to compensate $MoO_4^{2-}$ entities strongly decreases when $B_2O_3$ concentration increases and the $[Ca^{2+}]/[Na^+]$ concentrations ratio in depolymerized regions of glass structure (Fig. 1) increases which could explain the evolution of the crystallization tendency [5]. We recently confirmed this explanation by studying directly the effect on the crystallization behavior during melt cooling of changing the Ca/Na concentration ratio around $MoO_4^{2-}$ entities by changing the concentration ratio $Z = [CaO]/([CaO] + [Na_2O])$ from 0 (calcium-free sample) to 0.5 (sample with as much CaO as $Na_2O$) for another Mo-bearing soda-lime borosilicate glass composition 64.76 $SiO_2$–10.48 $B_2O_3$–13.68 $Na_2O$–8.43 CaO–2.5 $MoO_3$ (in mol%) [37].

Fig. 7 shows that $\delta_{iso}$ and Pq $^{23}Na$ NMR parameters significantly decreases when $B_2O_3$ concentration increases. Thus, contrary to the $M_x$ series, the distribution of $Na^+$ cations through the glassy network significantly changes when increasing amounts of boron are introduced in $B_y$ glasses. The comparison of $\delta_{iso}$ and Pq parameters of $B_y$ glasses with those of sodium silicate (SiNa), sodium calcium silicate (SiNaCa), SiNaMo and two borate (B0.2Na, B0.7Na) reference glasses clearly reveals that when $B_2O_3$ concentration increases, $Na^+$ cations moves from a position near NBO to a position near $BO_4^-$ units as charge compensator inducing both an increase of the d(Na–O) distance and a decrease of Pq because of the decrease of the local negative charge on oxygen atoms in the neighborhood of $Na^+$ cations. Indeed, in silicate and borate crystalline phases containing sodium, the decrease of $\delta_{iso}(^{23}Na)$ is known to be correlated with the increase of d(Na–O) [35,38,39].

In agreement with the XRD results obtained for the $B_y$ quenched disk samples (Fig. 9), Raman spectra of the same samples show

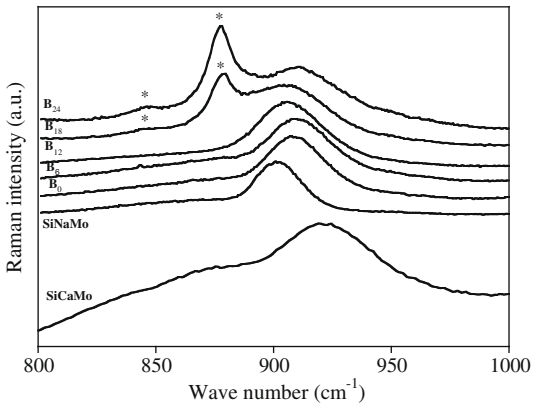


**Fig. 10.** Evolution of Raman spectra of $B_y$ samples. For comparison the spectra of SiNaMo and SiCaMo reference glasses are also shown. ∗: Vibration bands due to $CaMoO_4$ crystals in $B_y$ samples. Spectra have not been corrected for temperature and frequency dependent scattering intensity [45].

that the crystallization of $CaMoO_4$ is also detected when $y > 12$ mol% (Fig. 10). Contrary to Raman spectra of samples of the $M_x$ series (Fig. 4), the position of the band associated with the Mo–O symmetric stretching vibration only slightly varies when $B_2O_3$ concentration increases which indicates that the mean environment of $MoO_4^{2-}$ entities is only slightly modified and remains charge compensated both by $Na^+$ and $Ca^{2+}$ cations. This result could be explained by the fact that the depolymerized regions in which are located $MoO_4^{2-}$ entities (Fig. 1) become progressively depleted both in sodium (because of the charge compensation of $BO_4^-$ units by $Na^+$ cations, Fig. 8) and in calcium (because of $CaMoO_4$ crystallization, Fig. 9).

## 6. Conclusion

The structural study of two series of $SiO_2$–$B_2O_3$–$Na_2O$–CaO–$MoO_3$ glasses prepared by increasing either $MoO_3$ or $B_2O_3$ contents reveals two main points. The introduction of increasing $MoO_3$ contents induces an increase of the proportion of $Q_4$ units showing that this oxide acts as a reticulating agent on the silicate network whereas both the proportion of $BO_4^-$ units and the distribution of $Na^+$ cations are not significantly modified. The introduction of increasing $B_2O_3$ amounts strongly modifies the distribution of $Na^+$ cations within the glass network which could explain the evolution of the nature of molybdates that can crystallize during melt cooling ($CaMoO_4$ at the expense of $Na_2MoO_4$ [5]).

## Acknowledgments

The authors gratefully acknowledge M. Magnin (CEA Marcoule, France) for the preparation and the recording of the Raman spectrum of SiCaMo reference glass.

## References

[1] G. Calas, M. Le Grand, L. Galoisy, D. Ghaleb, J. Nucl. Mater. 322 (2003) 15–20.
[2] D. Caurant, P. Loiseau, O. Majérus, V. Aubin-Chevaldonnet, I. Bardez, A. Quintas, Glasses, Glass–Ceramics and Ceramics for Immobilization of Highly Radioactive Nuclear Wastes, Nova Science Publishers., Hauppauge, New York (USA), 2009.
[3] R.J. Short, R.J. Hand, N.C. Hyatt, Mater. Res. Soc. Symp. Proc. 757 (2003) 141–146.
[4] C. Cousi, F. Bart, J. Phallipou, J. Phys. IV France 118 (2004) 79–83.
[5] D. Caurant, O. Majérus, E. Fadel, M. Lenoir, C. Gervais, O. Pinet, J. Am. Ceram. Soc. 90 (2007) 774–783.
[6] R.J. Short, R.J. Hand, N.C. Hyatt, G. Möbus, J. Nucl. Mater. 340 (2005) 179–186.
[7] F. Farges, R. Siewert, G.E. Brown, A. Guesdon, G. Morin, Can. Mineral. 44 (2006) 731–753.
[8] N. Sawaguchi, T. Yokokawa, K. Kawamura, Phys. Chem. Glasses 37 (1996) 13–18.
[9] J. Aubry, D. Burnel, C. Gleitzer, in: Masson (Ed.), Compléments au nouveau traité de Chimie Minérale, Molybdène, vol. 5, Paris, France, 1976, pp. 78–113.
[10] G.J. McCarthy, J.G. Pepin, D.E. Pfoertsch, D.R. Clarke, Ceramics in nuclear waste management. in: Proceedings of an International Symposium. Cincinnati, April 1979, pp. 315–320.
[11] R. Do Quang, V. Petitjean, F. Hollebecque, O. Pinet, T. Flament, A. Prod'homme, Waste Management 2003 Symposium, Tucson, AZ, E-text: <www.wmsym.org/abstracts/2003/pdfs/92.pdf>.
[12] N. Henry, P. Deniard, S. Jobic, R. Brec, C. Fillet, F. Bart, A. Grandjean, O. Pinet, J. Non-Cryst. Solids 333 (2004) 199–205.
[13] R.J. Short, R.J. Hand, N.C. Hyatt, Mater. Res. Soc. Symp. Proc. 807 (2004) 169–174.
[14] A. Horneber, B. Camara, W. Lutze, Mater. Res. Soc. Symp. Proc. 11 (1982) 279–288.
[15] B. Camara, W. Lutze, J. Lux, in: C.J.M. Northrup (Ed.), Scientific Basis for Nuclear Waste Management II, Plenum Press, New York, 1979, pp. 93–102.
[16] I.D. Brown, R.D. Shannon, Acta Crystallogr. A A29 (1973) 266.
[17] L. Pauling, J. Am. Chem. Soc. 51 (1929) 1010.
[18] L. Galoisy, L. Cormier, S. Rossano, A. Ramos, G. Calas, P. Gaskell, M. Le Grand, Mineral. Mag. 64 (2000) 207–222.
[19] B. Bridge, N.D. Patel, J. Mater. Sci. 21 (1986) 1187–1205.
[20] S. Muthupari, G.U. Kulkarni, K.J. Rao, Bull. Mater. Sci. 17 (1994) 1029–1037.
[21] A. Kuzmin, J. Purans, J. Phys. IV France 7 (1997). C2-971–C2-973.
[22] G. Poirier, F.S. Ottoboni, LNSL 2007 Activity Report. (<http://www.lnls.br/ar2007/web/>).

[23] F.A. Cotton, M. Wing, Inorg. Chem. 4 (1965) 867–873.
[24] F.D. Hardcastle, I.E. Wachs, J. Raman Spectrosc. 21 (1990) 683–691.
[25] S. Kroeker, I. Farnan, S. Schuller, T. Advocat, Mater. Res. Symp. Proc. 1124 (2009) 153–159.
[26] M. Magnin, S. Schuller, D. Caurant, O. Majérus, D. de Ligny, C. Mercier, in: A. Cozzi, T. Ohji (Eds.), Ceramic Transactions, vol. 207, The American Ceramic Society, Wiley, 2009, pp. 59–68.
[27] F. Angeli, M. Gaillard, P. Jollivet, T. Charpentier, Chem. Phys. Lett. 440 (2007) 324–328.
[28] B. Bureau, G. Silly, J.Y. Buzaré, C. Legein, D. Massiot, Solid State Nucl. Magn. Res. 14 (1999) 181–190.
[29] G. Czjzek, J. Fink, F. Götz, H. Schmidt, J.M. Coey, J.P. Rebouillat, A. Liénard, Phys. Rev. B 23 (1981) 2513–2530.
[30] R.J. Landry, J. Chem. Phys. 48 (1968) 1422–1423.
[31] V. Aubin-Chevaldonnet, D. Gourier, D. Caurant, S. Esnouf, T. Charpentier, J.M. Costantini, J. Phys. Condens. Matter 18 (2006) 4007–4027.
[32] E. Sarantopoulou, C. Raptis, S. Ves, D. Christofilos, G.A. Kourouklis, J. Phys. Condens. Matter 14 (2002) 8925–8938.
[33] V.P. Mahadevan Pillai, T. Pradeep, M.J. Bushiri, R.S. Jayasree, V.U. Nayar, Spectrochim. Acta A 53 (1993) 867–876.
[34] D. Massiot, F. Fayon, M. Capron, I. King, S. Le Calvé, B. Alonso, J.-O. Durand, B. Bujoli, Z. Gan, G. Hoatson, Magn. Reson. Chem. 40 (2002) 70–76.
[35] F. Angeli, T. Charpentier, P. Faucon, J.C. Petit, J. Phys. Chem. B 103 (1999) 10356–10364.
[36] A. Quintas, T. Charpentier, O. Majérus, D. Caurant, J.L. Dussossoy, P. Vermaut, Appl. Magn. Reson. 32 (2007) 613–634.
[37] M. Magnin, S. Schuller, F. Angeli, D. Caurant, O. Majérus, D. de Ligny, in: Proceedings of the International Conference Global 2009, Paris, France, 6–11 September, 2009, paper 9288.
[38] A.M. George, S. Sen, J.F. Stebbins, Solid State Nucl. Magn. Reson. 10 (1997) 9–17.
[39] K.J.D. Mackenzie, M.E. Smith, Multinuclear Solid-State NMR of Inorganic Materials, Pergamon Materials Series, Elsevier Science, Oxford UK, 2002.
[40] (a) I.D. Brown, D. Altermatt, Acta Crystallogr. B 41 (1985) 240–244;
(b) I.D. Brown, D. Altermatt, Acta Crystallogr. B 41 (1985) 244–247.
[41] G.N. Greaves, S. Sen, Adv. Phys. 56 (2007) 1–166.
[42] K.G. Bramnik, H. Ehrenberg, Z. Anorg. Allg. Chem. 630 (2004) 1336–1341.
[43] Y.G. Petrosyan, E.V. Tkachenko, V.M. Zhukovskii, Neorg. Mater. 11 (1975) 1618–1621.
[44] T.M. Yanushkevich, V.M. Zhukovskii, Zh. Neorg. Khim. 18 (1973) 2234–2237.
[45] D.R. Neuville, B.O. Mysen, Geochim. Cosmochim. Acta 60 (1996) 1727–1737.